

International Conference on Space Optics—ICSO 2014

La Caleta, Tenerife, Canary Islands

7–10 October 2014

Edited by Zoran Sodnik, Bruno Cugny, and Nikos Karafolas



Dimensional stability of metal optics on nickel plated AlSi40

Jan Kinast

Kevin Grabowski

Ralf-Rainer Rohloff

Stefan Risse

et al.



DIMENSIONAL STABILITY OF METAL OPTICS ON NICKEL PLATED ALSI40

Jan Kinast^{1,2}, Kevin Grabowski¹, Andreas Gebhardt¹, Ralf-Rainer Rohloff³, Stefan Risse¹, Andreas Tünnermann^{1,2}

¹ *Fraunhofer Institute for Applied Optics and Precision Engineering IOF, Albert-Einstein-Str. 7, 07745 Jena, Germany.*

² *Friedrich Schiller University of Jena, Institute of Applied Physics, Abbe School of Photonics, Albert-Einstein-Str. 15, 07745 Jena, Germany.*

³ *Max Planck Institute for Astronomy MPIA, Königstuhl 17, 69117 Heidelberg, Germany.*

I. INTRODUCTION:

Ultra precise mirrors are particularly useful for space applications and scientific instrumentations for large telescopes, covering a highly variable temperature range. There are a variety of temperature ranges to be considered for metal optics: cryogenic instruments, applications under fluctuating ambient conditions (e.g. -40 °C – 60 °C) and applications under controlled operating temperatures (e.g. 20 °C ± 1 K). The dimensional stability of the applied materials is crucial for the optical performance at the addressed temperature range. Suitable thermal treatments as well as an athermal behavior of the applied materials are key issues for minimizing plastic and elastic shape changes of mirrors. Particularly SiC materials or low expansion glass ceramics, like Zerodur[®] or ULE[®] offer good preconditions, but also metals are able to achieve a good cost/performance ratio. Diamond turned Al6061 is a dimensionally stable material for metal optics for IR-applications [1]. Amorphous electroless nickel (NiP) as a polishing layer enables applications in the shorter wavelength region up to the UV spectral range [2]. But, operating temperatures different from ambient temperature lead to disadvantageous bimetallic bending due to different coefficients of thermal expansion (CTE) of Al6061 and NiP [3]. For minimizing the elastic shape changes, the CTE can be matched by selecting the chemical compositions of the used materials. In the case of the substrate, composite materials like aluminum-beryllium were investigated with the aim of matching the CTE of NiP [4-6]. This paper presents the approach of employing silicon particle reinforced aluminum materials with approx. 39 – 43 % Si (AlSi). The obtained CTE data show that different operating temperatures require different material combinations to achieve minimized elastic bimetallic bending. Furthermore, plastic shape changes of the applied materials must be prevented completely. Thermal treatments for AlSi materials, avoiding plastic shape changes at the relevant operating temperature over the lifetime of the optics, were investigated. It is shown that the dimensional stability of AlSi composites is a major challenge due to thermal mismatch stresses of the two phases, aluminum and silicon. A suitable thermal treatment method of AlSi is described. The stabilization mechanism is correlated to interferometric analyses of mirrors and TEM analyses of different heat-treated samples made of the same materials. The long-term stability of AlSi is shown by interferometric analyses after 32 months of storage at ambient temperature.

II. TEST PRINCIPALS:

A. Materials

Aluminum substrates

The aluminum alloy Al6061 is widely used to fulfill requirements for metal optics to be used in the IR spectral range [7,8]. This alloy contains a 0.8 wt% – 1.2 wt% share of magnesium and a 0.4 wt% – 0.8 wt% share of silicon as major alloying elements. Due to the polycrystallinity, the achievable roughness value of diamond turned Al6061 is limited [1,8,9]. For applications in the visible spectral range, roughness values of lower than 2 nm root mean square (RMS) are necessary. NiP with a phosphorous content higher than 10.5 wt% is a suitable coating material for several polishing processes [10]. For applications at temperatures different from ambient room temperature, the bimetallic bending caused by the different coefficients of thermal expansion (CTE) of both materials is detrimental. Thus, a thermally matched aluminum material containing approx. 39 – 43 wt% Si is investigated. The material is compounded via a rapid solidification process followed by hot isostatic pressing. The resulting AlSi material is a silicon particle reinforced aluminum material as shown in Fig. 1.

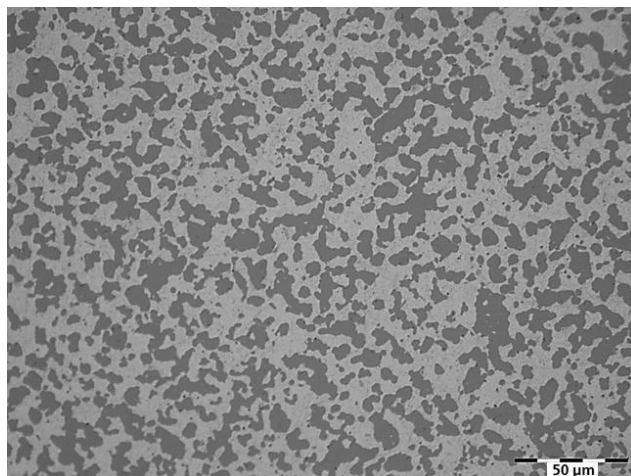


Fig. 1. Microstructure of AlSi containing a 42 wt% share of silicon (dark grey).

Thermal treatments of such materials lead to elastic deformations. Furthermore, plastic deformations in the aluminum matrix may be possible that are caused by different CTE values of the two phases. Plastic deformations, occurring between ambient temperature and the operating temperature, need to be prevented completely. Otherwise, the material cannot be used as substrate for ultra-precise metal optics. Therefore, several thermal treatment steps of AlSi are necessary throughout the entire manufacturing chain in order to stabilize the material dimensionally. It is generally accepted that the microstructure of particle reinforced materials influences the thermo-mechanical behavior [11]. In this work, two AlSi alloys (A and B) with different microstructures were analyzed in terms of elastic and plastic shape changes. The aim of the investigation is to find materials with a dimensional stable behavior. AlSi_A and AlSi_B differ in the particle size of silicon and in their chemical composition. AlSi_B has a higher share of silicon and a coarser-grained structure.

Electroless NiP

NiP is an alloy containing nickel and supersaturated phosphorus. It is a coating, which can be deposited on metallic surfaces in a water-based electrolyte at elevated temperatures through autocatalytic chemical reactions. Electrons, which are required for reducing the adsorbed nickel ions on the surface, are generated in the electrolyte itself. Therefore, the chemical process enables uniformly distributed layers over the whole substrate. The phosphorous content influences almost all properties of the alloy, e.g. hardness, crystallinity, and CTE [12,13]. For tailoring these properties, the phosphorous content can be manipulated via the deposition parameters of the used electrolyte [14]. NiP with a phosphorous content higher than 10.5 wt% is referred to as X-ray amorphous [15]. Therefore, NiP is machinable via diamond turning techniques to a roughness lower than 2 nm RMS [10]. Several polishing techniques are possible to remove the resulting turning marks. Applying computer-aided polishing with sub-aperture tools, a roughness lower than 1 nm RMS is achievable [2]. Furthermore, local figuring techniques like Magnetorheological Finishing (MRF) enable the deterministic figure correction of NiP-layered metal surfaces [16].

B. Analysis of the coefficient of thermal expansion

For minimizing the bimetallic bending due to the different CTE values of substrate and polishable layer, the knowledge of the CTE is crucial. CTE matching enables material combinations with minimized elastic shape changes that are caused by temperature changes. For CTE analyses, cylinders made of AlSi and sheets made of NiP are prepared. The aluminum samples require dimensions of 12 mm in length and 6 mm in diameter, while the NiP sheets have to be thicker than 150 μm , with a length of 12 mm. Whereas AlSi samples can be fabricated comparatively easily, the manufacturing of suitable NiP samples is a challenging task. To realize debris-free NiP sheets (12 mm \times 6 mm), ps-laser cutting and subsequent polishing steps were used. Samples are analyzed with a push-rod dilatometer DIL 402 C by NETZSCH. The length change of the samples is analyzed in the temperature range between -180 $^{\circ}\text{C}$ and 100 $^{\circ}\text{C}$ in a helium purged atmosphere. Using equation (1) the CTE is calculated as a function of temperature, where L is the length and T is the temperature of the sample.

$$CTE = \frac{1}{L} \times \frac{dL}{dT} \quad (1)$$

A sample placement of prepared NiP in the dilatometer is shown in Fig. 2.

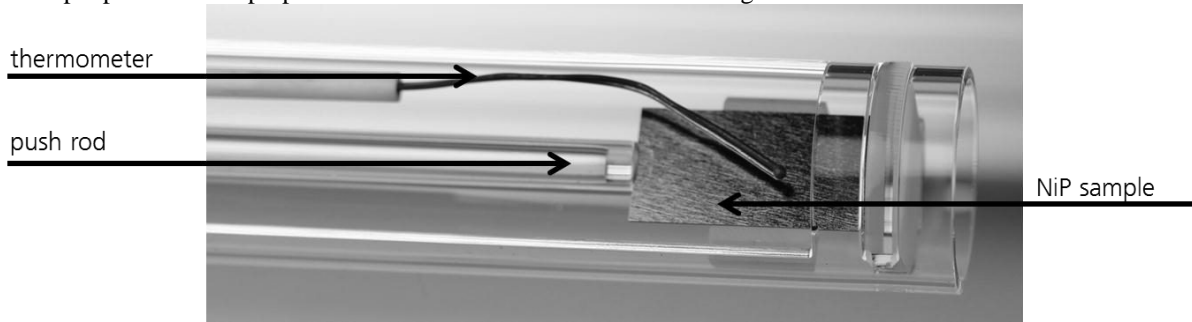


Fig. 2. NiP sample in a push-rod dilatometer DIL 402 C by NETZSCH.

The reproducibility of the developed CTE analyses is $\pm 0.15 \times 10^{-6} \text{ K}^{-1}$. Fig. 3 shows CTE data of Al6061, AlSi containing a 39 wt% share of silicon (AlSi39), AlSi42, and NiP containing an 11 wt% share of phosphorus (NiP11) in a temperature range of $-180 \text{ }^\circ\text{C}$ to $100 \text{ }^\circ\text{C}$. The silicon content of the substrate and the CTE, respectively, are matched to the CTE of the polishable NiP layer.

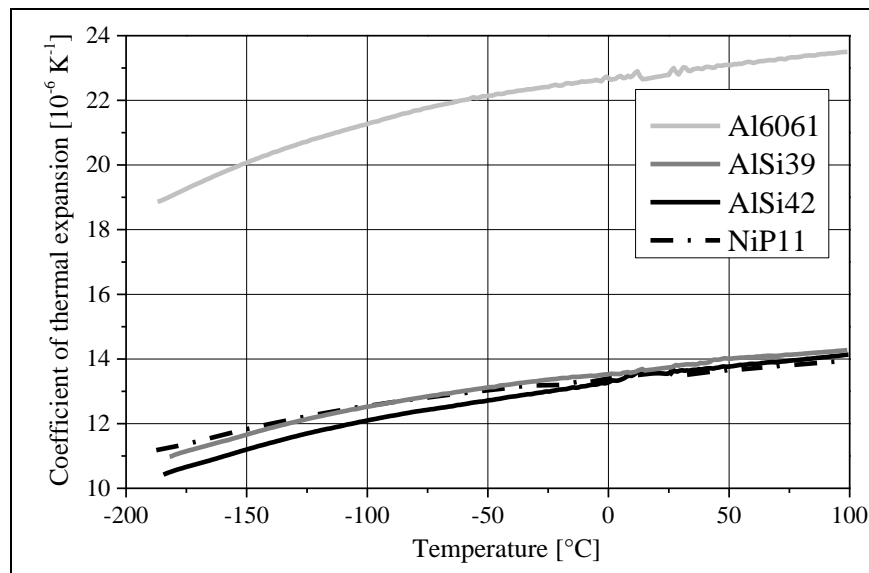


Fig. 3. Coefficients of thermal expansion of Al6061, AlSi39, AlSi42, and NiP11 in a temperature range between $-180 \text{ }^\circ\text{C}$ and $100 \text{ }^\circ\text{C}$.

For applications under fluctuating ambient conditions, AlSi42 shows an average thermal mismatch of $< 0.1 \times 10^{-6} \text{ K}^{-1}$ compared to the coating. Cryogenic applications require lower silicon contents and a higher CTE to match the CTE of NiP between $20 \text{ }^\circ\text{C}$ and cryogenic temperatures. The tailored CTE of AlSi39 leads to an average CTE mismatch of $< 0.1 \times 10^{-6} \text{ K}^{-1}$ in a temperature ranging from $-187 \text{ }^\circ\text{C}$ to $20 \text{ }^\circ\text{C}$. This fact clarifies that different operating temperatures require different material combinations. Matching the CTE of substrate and polishable layer minimizes the elastic shape change due to different thermal conditions.

C. Dimensional Stability Validation

The optical quality, described by roughness and shape deviation of metal optics, must remain constant over the lifetime of the optical system. For avoiding plastic deformations of nickel plated AlSi, the substrate material has to be stabilized prior and after cutting processes. Further treatment steps are necessary after the plating and figuring procedures. In principle, the operating temperature defines the thermal treatment that is necessary. The essential part dominating the structural mechanical behavior under the influence of temperature and time is given by the mirror bulk material itself. Therefore, research is focused on the dimensional stability of the substrate materials AlSi_A and AlSi_B. The influence of the silicon particle size of AlSi on the dimensional stability is investigated for fluctuating ambient ($-40 \text{ }^\circ\text{C}$ to $60 \text{ }^\circ\text{C}$) and cryogenic ($-196 \text{ }^\circ\text{C}$) operating temperatures. Initially, the stabilization characteristics of sample mirrors are investigated by experimental verification of the remaining figure deformation after thermal treatment. For understanding the stability

behavior, transmission electron microscopy (TEM) was used to identify microstructural modifications. As a result, a model of an obvious strengthening mechanism could be established.

Analysis of the dimensional stability of mirrors via interferometry

In order to evaluate the plastic dimensional stability of AlSi_A and AlSi_B, the materials are annealed at a temperature of > 300 °C. From this raw material, mirrors with a diameter of 48 mm and a height of 15 mm are prepared via diamond turning. The shape deviation of the mirrors is analyzed by an interferometric technique. The used interferometer is a ZYGO DynaFiz™ with a clear aperture of 6” and a transmission flat with an accuracy of $\lambda/20$ at 633 nm. For evaluating the dimensional stability of AlSi in a temperature range between -40 °C and 60 °C, the mirrors were thermally cycled within the temperature range. After thermal treatment, the shape deviation is analyzed by interferometry at ambient temperature. The change in shape deviation is defined as the difference between two consecutive interferometric results. The procedure (step 5 and step 6), given in Table 1, is repeated up to 30 times (-40 °C to 60 °C) and up to six times (-196 °C to 20 °C) in the case of cryogenic investigations.

Table 1. Process steps of sample preparation and analysis of shape deviation changes.

step #	
1	rough machining of AlSi samples
2	annealing > 300 °C
3	diamond turning of AlSi mirrors
4	interferometry at ambient temperature
5	thermal cycle (-40 °C to 60 °C or -196 °C to 20 °C)
6	interferometry at ambient temperature

Fig. 4 shows that AlSi_B is dimensionally stable after one thermal cycle between -40 °C and 60 °C. Contrarily to the behavior of mirrors made of AlSi_B, mirrors made of AlSi_A show an increased shape deviation after several thermal cycles between -40 °C and 60 °C. After the first thermal cycle, the shape deviation increases by 22 nm RMS. Additional thermal cycles lead to a progressively smaller increase of shape deviation.

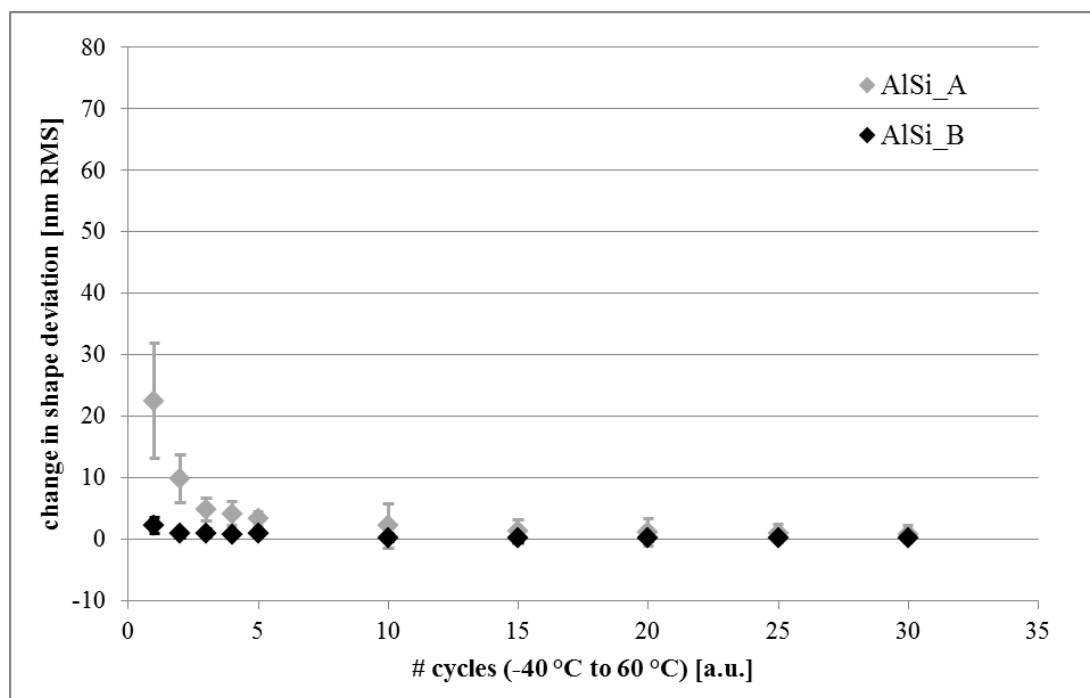


Fig. 4. Dimensional stability of AlSi_A and AlSi_B in a temperature range from -40 °C to 60 °C.

After 25 cycles, mirrors made of AlSi_A show a change in shape deviation lower than 1 nm RMS. AlSi_B is dimensionally stable in the addressed temperature range (-40 °C – 60 °C) after one cycle.

For cryogenic applications, the dimensional stability of AlSi_A and AlSi_B is investigated, too. In principle, the behavior of the plastic shape changes is similar to the investigations in the temperature range from -40 °C to 60 °C. After the first cryogenic cycle between -196 °C and 20 °C, both materials show an increased shape deviation, cf. Fig. 5.

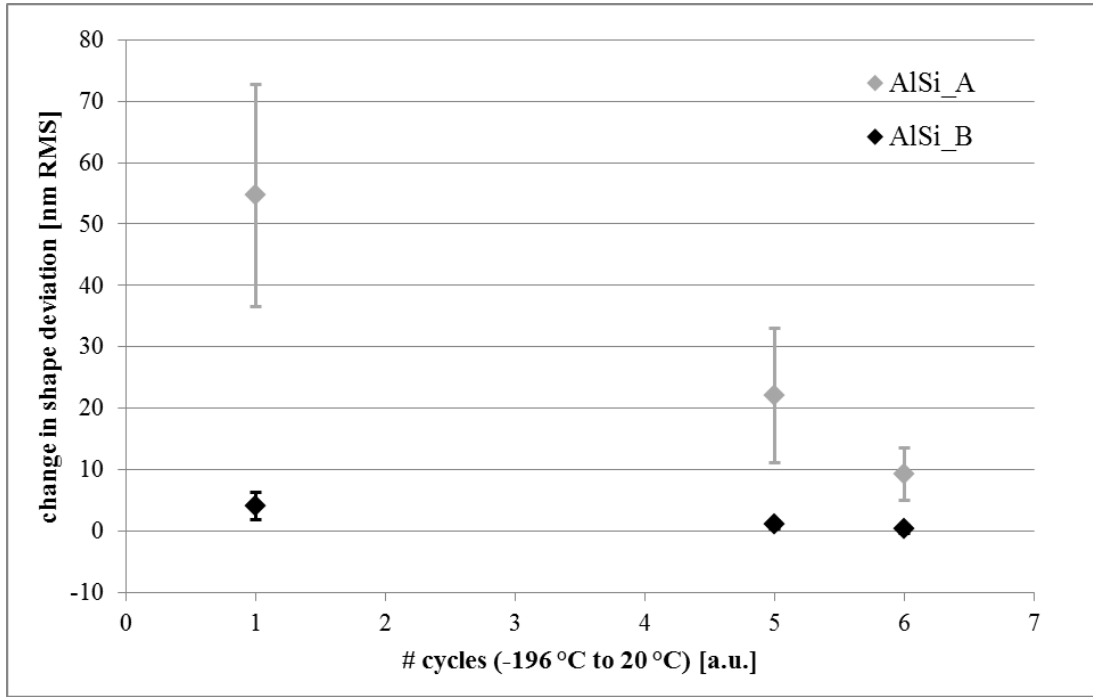


Fig. 5. Dimensional stability of AlSi_A and AlSi_B in a temperature range from -196 °C to 20 °C.

Additional cryogenic cycles of AlSi_A mirrors lead to a progressively smaller increase of shape deviation. AlSi_B mirrors show a dimensional stability after the first cryogenic cycle, while AlSi_A mirrors do not show a dimensional stability after up to six cryogenic cycles.

The long-time stability has been proven by interferometry after mirror storage at ambient temperature. After one year, the mirrors show almost the same shape of the optical surface. Therefore, both materials seem to be dimensionally stable, cf. Table 2. After 32 months, AlSi_A mirrors show a significant change in shape deviation with a high standard deviation of 7 nm RMS, which is caused by inhomogeneities of AlSi_A. AlSi_B mirrors show a slight change in shape deviation of 1.3 nm RMS, which represents the reproducibility of the interferometric analyses.

Table 2: Change in shape deviation of mirrors made of AlSi_A and AlSi_B after 6 cryogenic cycles, 12 months, and 32 months at ambient temperature.

material	after 6 cryogenic cycles	after 12 months at ambient T	after 32 months at ambient T
AlSi_A	9.3 ± 4.2 nm RMS	1.0 ± 0.6 nm RMS	7.2 ± 7.3 nm RMS
AlSi_B	0.3 ± 0.6 nm RMS	0.4 ± 0.5 nm RMS	1.3 ± 0.8 nm RMS

It is shown that the investigated AlSi_B mirror with the coarser-grained structure is dimensionally stable over a long time of several years. The relaxation temperature of aluminum proved to be higher than 20 °C, so that operating temperatures of lower than 20 °C do not lead to a relaxation. Therefore, a change in shape of mirrors made of AlSi_B is not expected at cryogenic usage.

Investigation of the strengthening mechanism via Transmission Electron Microscopy

For describing the different and convergent behavior of shape changes due to thermal treatments of both AlSi materials, a strengthening mechanism has to have been in effect. Thermal mismatch stresses due to thermal treatments, occurring on the microscale between the aluminum matrix and the silicon particles in AlSi, induce plastic deformations, which lead to a strengthening of the AlSi material. Additional thermal treatments usually lead to the same mismatch stresses, but the strengthened material is able to absorb more stresses elastically. This strengthening mechanism is called work hardening and is caused by the formation of dislocations and by the hindering of dislocation movements. To prove this theoretical model and to investigate the influence of the microstructure on the strengthening behavior, AlSi samples are analyzed by TEM. Four batches are analyzed regarding the formation of dislocations after several thermal treatments. AlSi_A and AlSi_B samples are used that underwent different thermal treatments. On the one hand, they are solely hot isostatic pressed samples, on the other hand they are samples, which are annealed at $> 300\text{ }^{\circ}\text{C}$ and then 30 times thermally cycled ($-40\text{ }^{\circ}\text{C}$ to $60\text{ }^{\circ}\text{C}$), and five times cryogenically cycled ($-196\text{ }^{\circ}\text{C}$ to $20\text{ }^{\circ}\text{C}$). The samples are prepared by dimple grinding using a "Gatan Dimple Grinder 656". They are electrochemically etched using a "Struers Tenupol-3" with $\text{CH}_4\text{O} - \text{HNO}_3$ solution (3:1) as etchant for minimizing parasitic heat influence. The resulting grains are thin enough ($< 100\text{ nm}$) to permit transmission of electrons. Fig. 6 shows representative results of TEM investigations of solely hot isostatic pressed AlSi samples.

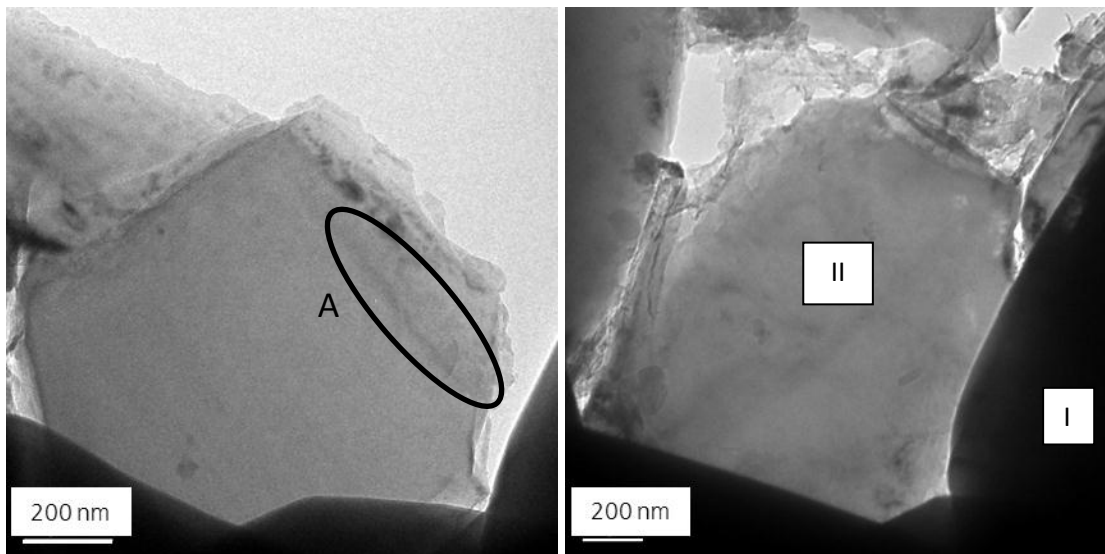


Fig. 6. AlSi_A (left) and AlSi_B (right) in the solely hot isostatic pressed state.

The contrast (Fig. 6; right: marked by I and II) is due to different thicknesses of the grains and can be attributed to the different etching behavior during the last preparation step. Caused by different atomic distances in the crystal lattice, stress fields are visible in transmission electron micrographs. AlSi_A and AlSi_B rarely exhibit stress fields (Fig. 6; left: marked by A). They do not show indications of plastic deformation like dislocations, stacking faults, or twins in the solely hot isostatic pressed state, cf. Fig. 6. In contrast, samples which are annealed, thermally cycled between $-40\text{ }^{\circ}\text{C}$ and $60\text{ }^{\circ}\text{C}$ 30 times, and five times cryogenically cycled ($-196\text{ }^{\circ}\text{C}$ to $20\text{ }^{\circ}\text{C}$) show a significant higher amount of dislocations as is shown in Fig. 7.

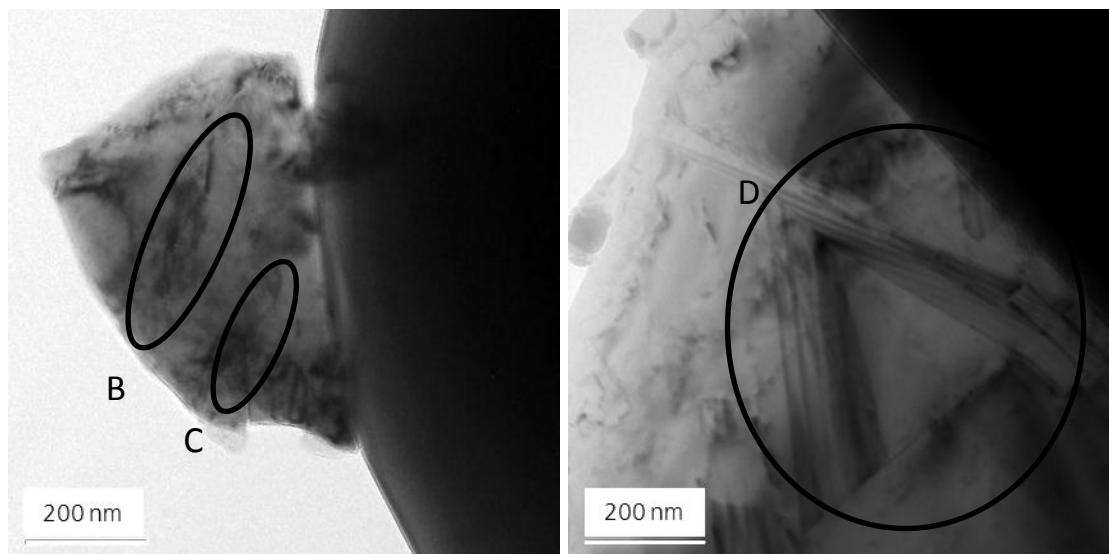


Fig. 7. AlSi_A (left) and AlSi_B (right) after annealing, thermal cycling (-40 °C to 60 °C), and cryogenic cycling (-196 °C to 20 °C).

Furthermore, stress fields are found in almost every grain of AlSi_A and AlSi_B. The CTE of aluminum and silicon differs by $20 \times 10^{-6} \text{ K}^{-1}$. These intrinsic stresses lead to plastic deformations and result in an irreversible shape change and a strengthening of AlSi due to thermal treatments. AlSi_A shows stress fields and dislocations (Fig. 7; left: marked by B and C). The dislocations are partially overlaid by elastic stress fields. All observed grains, a variety of such elastic stress fields and dislocations, have been investigated. In comparison to the solely hot isostatic pressed state, a significant increase of lattice defects is observed.

AlSi_B shows stress fields in each grain. Furthermore, indications of plastic deformation are visible. It is noteworthy that numerous twins and stacking faults were found, which indicate high stresses induced by the CTE mismatch of the aluminum matrix and silicon particles. Two stacking faults displayed in Fig. 7 (right: marked by D) indicate high induced stresses, generating dislocations and a strong strengthening mechanism. Accordingly, the reaction is indicative for the increased strength of AlSi_B depending on the more effective dimensional stabilization of the coarser-grained material. In summary, the interferometrical results of the sample mirrors made of AlSi_A and AlSi_B are confirmed via TEM analyses combined with a developed model of strengthening mechanism.

III. CONCLUSION:

This paper describes the dimensional stability of mirrors made of AlSi containing a 39 to 43 wt% share of silicon. Such substrate materials can be thermally matched to amorphous NiP layers. The CTE matching is adjustable through the chemical composition of the substrate material and depends on the operating temperature. Different particle sizes of silicon particle reinforced aluminum materials lead to different efficiency regarding the dimensional stabilization by thermal treatments. Coarser-grained AlSi alloys are stabilized more effectively. Dimensional long-term stability could be shown after 32 months at ambient temperature. The investigated strengthening mechanism of AlSi is confirmed via TEM analyses. Annealed and thermal cycled AlSi samples show a significant higher amount of dislocations, twins and stacking faults, which lead to a high dimensional stability of metal optics based on AlSi and work hardening. Well-defined thermal treatment procedures enable the usage of nickel plated AlSi40 optics for many applications at different operating temperatures.

ACKNOWLEDGEMENTS

Funding (grant no. 03WKCK1B) within the framework "Unternehmen Region - Innovative Regional Growth Core" from the Federal Ministry of Education and Research (BMBF) is gratefully acknowledged.

REFERENCES

- [1] D. Vukobratovich and J.P. Schaefer, "Large stable Aluminum Optics for Aerospace Applications," *Proceedings SPIE 8125: Optomechanics 2011: Innovations and Solutions*, 2011.
- [2] R. Steinkopf et al., "Metal mirrors with excellent figure and roughness," *Proceedings SPIE 7102: Optical Fabrication, Testing, and Metrology III*, 2008.
- [3] R.-R. Rohloff et al., "A novel athermal approach for high-performance cryogenic metal optics," *Proceedings SPIE 7739: Modern Technologies in Space- and Ground-based Telescopes and Instrumentation*, 2010.
- [4] M. Cayrel, R.A. Paquin, T.B. Parsonage, S. Stanghellini, and K. H. Dost, "Use of Beryllium for the VLT Secondary Mirror," *Proceedings SPIE 2857: Advanced Materials for Optical and Precision Structures*, 1996.
- [5] T. Parsonage, "New Technologies for Optical Systems Utilizing Aluminum Beryllium," *Proceedings SPIE 7018: Advanced Optical and Mechanical Technologies in Telescopes and Instrumentations*, 2008.
- [6] S. Say, J. Duich, C. Huskamp, and R. White, "Cost Effective Aluminium Beryllium Mirrors for Critical Optics Application," *Proceedings SPIE 8837: Material Technologies and Applications to Optics, Structures, Components, and Sub-Systems*, 2013.
- [7] F.J. Fuentes, A. Manescau, E. Cadavid, and V.S. de la Rosa, "Design, fabrication and testing of aluminium mirrors for cold optics of the IAC infrared camera," *Proc. SPIE 2227: Cryogenic Optical Systems and Instruments VI*, 26 – 32, 1994.
- [8] G.P.H. Gubbels, B.W.H. van Venrooy, A.J. Bosch, and R. Senden, "Rapidly solidified aluminium for optical applications," *Proceedings SPIE 7018: Advanced Optical and Mechanical Technologies in Telescopes and Instrumentation*, 70183A-1 – 70183A-9, 2008.
- [9] D. Vukobratovich, K. Don, R. Summer, et al., "Improved cryogenic aluminum mirrors," *Proceedings SPIE 3435: Cryogenic Optical Systems and Instruments VIII*, 1998
- [10] S. Risse et al., "Novel TMA telescope based on ultra-precise metal mirrors," *Proceedings SPIE 7010: Space Telescopes and Instrumentation 2008: Optical, Infrared, and Millimeter*, 701016-1 – 701016-8, 2010.
- [11] M. Gupta and E.J. Lavernia, "Effect of processing on the microstructural variation and heat-treatment response of a hypereutectic Al-Si alloy," *Journal of Materials Processing Technology* 54, 261 – 270, 1995.
- [12] W. Qin, "Microstructure and corrosion behaviour of electroless Ni-P coatings on 6061 aluminum alloys," *Journal of Coatings Technology and Research* 8 (1), 135 – 139, 2011.
- [13] D.L. Hibbard, "Electrochemically deposited nickel alloys with controlled thermal expansion for optical applications," *Proceedings SPIE 2542: Optomechanical and Precision Instrument Design*, 236 – 243, 1995.
- [14] H.R. Molla, H. Modarress, and M. Abdouss, "Electroless nickel-phosphorus deposition on carbon steel CK-75 and study of the effects of some parameters on properties of the deposits," *Journal of Coatings Technology and Research* 9 (2), 183 – 188, 2012.
- [15] N.M. Martyak et al., "Structure of electroless nickel coatings," *Plating and Surface Finishing*, 60 – 64, 1993.
- [16] M. Beier et al., "Fabrication of high precision metallic freeform mirrors with magnetorheological finishing (MRF)," *Proceedings SPIE 8884: Optifab 2013*, 88840S-1 – 88840S-14, 2013.